Available online at www.sciencedirect.com
SCIENCE DIRECT®
International Journal of Heat and Mass Transfer 48 (2005) 3363–3380
International Journal of HEAT and MASS TRANSFER
www.elsevier.com/locate/ijhmt

Features of convective heat transfer in heated helium channel flow

S. Gordeev *, V. Heinzel, V. Slobodtchouk

Forschungszentrum Karlsruhe GmbH, Postfach 3640, D-76021 Karlsruhe, Germany

Received 25 August 2004; received in revised form 11 January 2005

Abstract

The aim of the present work is to choose an optimal method for thermohydraulic calculation of the gas flow in channels with intense heating at the flow Reynolds number below 10,000. These conditions are typical of the cooling channels of the High-Flux-Test Module of the International-Fusion-Materials-Irradiation-Facility (IFMIF/HFTM). A low Reynolds number and a high heating rate can result in partial relaminarization of the initially turbulent flow, and hence in a decrease in the heat transfer. A number of turbulence models offered by the commercial STAR-CD code were tested on the basis of the comparison of the numerical predictions with experimental data. This comparison showed that the low-Reynolds-number k–ε turbulence models predict the heat transfer characteristics close to the experimental data. The k–ε linear low Reynolds number turbulence model of Lien was applied as more appropriate for the thermohydraulic analysis of the IFMIF high flux test module.

1. IFMIF operation conditions

The International Fusion Materials Irradiation Facility [1] is an accelerator-based D/Li neutron source. It is capable of producing neutrons at sufficient energy and intensity to test specimens of candidate materials up to full lifetime in nuclear fusion reactors. In the High Flux Test Module (Fig. 1) the damage rate of more than 20 dpa/fpy (iron) will be achieved in the volume of about 0.5 l. The HFTM test section contains rigs with the material specimens to be irradiated.

The design of the HFTM test section is basically determined by the requirements derived from the test objectives and from the features of the test machine. The main requirements can be summarised as follows:

- The available test volume should be used to the maximum possible degree, i.e. the packing density of the specimens in the test section should be as high as possible, and the volume occupied by structural parts, insulation, cooling channels, etc. should be as small as possible.
- The HFTM should principally allow the irradiation temperatures between about 250 and 1000 °C.
- The deviations from the target temperature within a rig should be as low as possible. A range of ±10–15 °C is considered as reasonable.
- To compensate the axial nuclear heating gradient in rigs and to keep the irradiation temperature constant during beam intensity variations and beam-off periods electrical heating is required.

* Corresponding author. Fax: +49 7247 82 3718.
E-mail address: gordeev@irs.fzk.de (S. Gordeev).

0017-9310/$ - see front matter © 2005 Elsevier Ltd. All rights reserved.
doi:10.1016/j.ijheatmasstransfer.2005.02.023

Nomenclature

A	cross-section area
c_p	specific heat at constant pressure
D, D_h	diameter, hydraulic diameter
g	acceleration of gravity
G	mean mass flux, m'/A
h	thermal enthalpy
k	turbulent kinetic energy
L	length
m'	mass flow rate
P	piezometric pressure
q	heat flux
r	radial coordinate
R	tube wall radius
T	absolute temperature
U, u	mean velocity components
u'	fluctuating velocity
$\rho\overline{u_i'u_j'}$	Reynolds stress tensor
u_τ	friction velocity, $\sqrt{\tau_w/\rho}$
x	axial coordinate
y	wall distance coordinate
z	axial coordinate measured from nominal start of heating

Non-dimensional quantities

K	acceleration parameter
Nu	local Nusselt number
Pr	Prandtl number
q^+	heat flux parameter
R_t	turbulent Reynolds number
Re	Reynolds number
y^+	wall distance coordinate, yu_τ/v

Greek symbols

ε	dissipation of turbulent kinetic energy
λ	thermal conductivity
μ	molecular viscosity
μ_t	turbulent viscosity
v	kinematic viscosity
ρ	density
τ_w	wall shear stress
ω	turbulence frequency

Subscripts

b	bulk
heat	heating
i, in	inlet, inner
out	outlet, outer
t	turbulent
w	wall

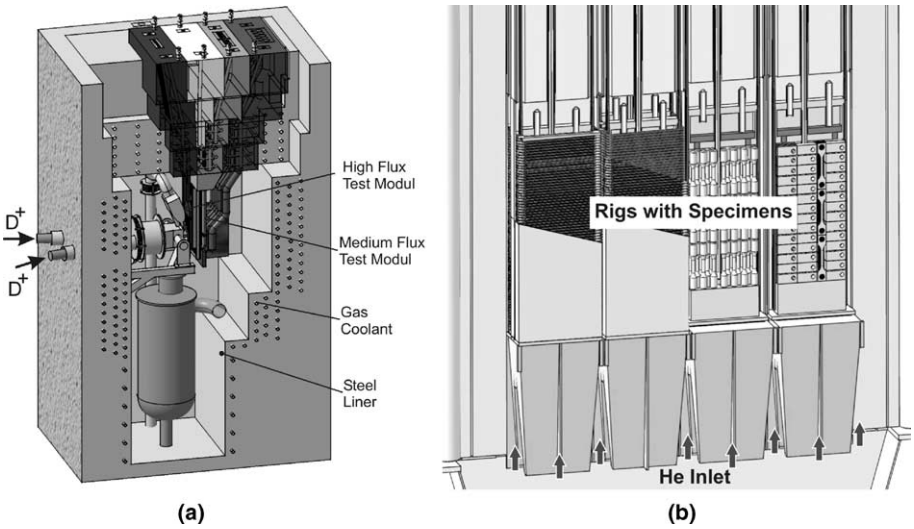

Fig. 1. IFMIF Test cell (a) and High Flux Test Module (b).

The HFTM is cooled by helium at low pressure (0.3 MPa at the inlet) and low temperature (about 50 °C at the inlet). Helium was selected because it is inert, does not undergo nuclear and chemical reactions, and has—compared to other gases—a high cooling capacity. Low pressure is important to avoid excessive mechanical loads on the structures, although a higher pressure would be desirable to reduce the coolant velocity and hence, the pressure loss. The low inlet temperature is necessary to realise the low level of the

irradiation temperature. The temperature rise of the coolant inside the HFTM should be in the range of 30–50 °C to reduce the axial temperature gradient. The flow direction is upward in the test volume.

The test section itself consists of a container with an inner cross-section of 203×51 mm^2. The container is divided into four compartments by stiffening plates serving to stabilise the container walls. Each compartment is filled with three rigs. The rigs have a rectangular cross-section with the outer dimensions of 49×16 mm^2. Cooling channels are provided at all sides of the rigs with the width of 1.0 mm at the large sides and of 0.5 mm at the small sides. Small vertical ribs at the corners of the rigs assure the dimensions of the cooling channels. The test section is heated, first of all, by nuclear heating and additionally by electrical heaters. The restrictions imposed on the He flow heating and on the He pressure result in a low Reynolds number in the cooling channels: $Re < 10{,}000$. So, the test section operation conditions create prerequisites for the phenomenon called flow relaminarization discussed below.

2. Flow relaminarization

2.1. Causes and mechanism of relaminarization

An intense heating of the gas turbulent flow can result in its relaminarization, i.e. the initially turbulent flow may become either partially or completely laminarized. The relaminarization phenomenon is a consequence of significant fluid property variations. It is known that the gas dynamic viscosity increases with the temperature rise. The viscous shear stress also increases in the near wall region where the flow temperature is close to the wall temperature that suppresses the turbulent energy production. Under the relatively low Reynolds (Re) number at the inlet to the channel (4000–6000) the local Re number gradually decreases along the heated section and can fall below the critical value resulting in "reverse transition" from the turbulent flow to the laminar one.

The transition from the turbulent to the laminar flow may begin at considerably higher Re numbers. The general effect of the intense heating of the gas is a reduction of the gas density causing flow acceleration in the central core, which leads to a decrease in the turbulence intensity in the flow. It is known [2] that in a turbulent flow the turbulence production is concentrated on the boundary of the so-called viscous sub-layer. The main mechanism of the turbulence production is a "burst-sweep" process. This process consists of several phases including (a) an eddy deceleration or ejection, (b) a rapid acceleration or sweep, and (c) a relatively quiescent process, or more gradual deceleration following the sweep. The flow acceleration modifies the burst phenomenon decreasing the burst frequency (or eliminating it altogether) and thus affects the turbulence production.

One of the explanations of the influence of the acceleration on the turbulence is the following. At the rapid flow acceleration a large axial velocity gradient causes an increase in viscous shear stress in the near wall region. The turbulence dissipation rate surpasses the turbulent production rate and the turbulence begins to decay. This decay can be seen in a reduction in the Reynolds stress. As long as the flow acceleration is maintained, the sequence of events would be self-propagating since the reduction in the Reynolds stress would lead to a further reduction in the production/dissipation ratio [3].

In their investigations Narahimba and Sreenivasan [4] concluded that the reason for the flow relaminarization under its acceleration is not only the growth of the turbulence dissipation but also the domination of the pressure forces over the slowly responding Reynolds stresses. They proposed a two-layer model of the flow comprised of a viscous inner layer and an inviscid outer layer to explain the mechanism of the relaminarization. The turbulence in the outer layer is distorted rather than destroyed by the acceleration. The residual upstream turbulence will persist, but no longer play a role in the relevant dynamics of the flow. The turbulence intensity in the flow direction goes down and the turbulence intensity in the normal direction goes up, so the Reynolds stress is nearly frozen. Simultaneously a new viscous layer develops in which the initial turbulence decays due to viscous dissipation. The burst-sweep phenomena are suppressed and so there is a weak or no interaction between the two layers.

Under these conditions the Reynolds number is not the main criterion of the turbulence and the relaminarization process can take place at a higher Reynolds number of the flow than the critical one.

2.2. Criteria for relaminarization

The consequence of the relaminarization is a substantial reduction in the heat transfer coefficient and an increase in wall temperature. If this fact is not taken into consideration then using the empirical correlations for the calculations one can obtain a significantly lower wall temperature than the real one. For engineering purposes one needs design criteria to predict when it is imminent.

In the studies of heat transfer to accelerated pipe flows a non-dimensional acceleration parameter K [5] is recommended as a criterion for relaminarization:

$$K = \frac{v}{U_b^2}\frac{dU_b}{dx}$$

where v is kinematic viscosity of a fluid and U_b is a bulk velocity.

This criterion can also be represented based on the non-dimensional heating intensity q^+ and the bulk Reynolds number as follows:

$$K = \frac{4q^+}{Re}\left(\frac{T_i}{T_b}\right)$$

where T_i and T_b are the inlet and bulk temperature, respectively, and

$$q^+ = \frac{q_w}{G \cdot c_{p,i} \cdot T_i}$$

q_w is the heat flux from a wall to the gas, G is the mass flow velocity (kg/m^{2}s), $c_{p,i}$ is the gas specific heat at the inlet temperature.

If the acceleration parameter K is less than 2×10^{-6}, the flow remains turbulent, while for higher values of K the relaminarization occurs [6]. The criterion for relaminarization can be expressed in terms of q^+, then the relaminarization begins at $q^+ \geqslant 0.003$ (however, this limit varies with the Reynolds number).

The typical value of q^+ is in the range of 0.0015–0.0025 for the cooling channels of the IFMIF/HFTM at samples temperature of 650–1000 °C. This means that the complete flow relaminarization will not take place. However, an intense heating of the gas flow can result in noticeable thickening in the viscous layer, in the reduction of the heat transfer coefficient, and in the temperature rise in samples and structure. Taking into account that the temperature of the samples should be kept quite constant in the predefined range (the acceptable temperature variations of ±10–15 K from the target value) it is necessary to determine exactly the influence of the relaminarization effect on the gas flow in the cooling channels.

2.3. Dependence of gas properties on temperature in empirical correlations

For preliminary estimations of the heat transfer coefficient in the channel, one can use the empirical correlations based on the experimental data. McEligot [6] has analysed a number of such correlations in which attempts are made to take into account the dependence of the flow properties on temperature. The discrepancy between the experimental data and the predictions of these correlations is in the range of 10–25% or more. The applicability of some of them is restricted by the value of the Prandtl and Reynolds numbers, by the shape of the channel and its length, by the type of the boundary conditions and so on. The following correlation is recommended as more appropriate for the calculations of the Nusselt number:

$$Nu = 0.021 \cdot Re_b^{0.8} \cdot Pr_b^{0.55} \cdot \left[\left(\frac{T_w}{T_b}\right)^{-0.4} + 0.85 \cdot \frac{D}{x}\right]$$

Here D is the hydraulic diameter of the channel, x is its current length, and the index b denotes the parameter calculated at the bulk temperature.

Gnielinski [7] proposed the following correlation for the calculation of the Nusselt number for transition flows with $2300 < Re < 10^4$:

$$Nu = (1-\gamma) \cdot Nu_L + \gamma \cdot Nu_T.$$

Here $\gamma = (Re - 2300)/(10^4 - 2300)$, Nu_L and Nu_T are the Nusselt numbers calculated for the laminar flow at $Re = 2300$ and the turbulent flow at $Re = 10^4$, respectively. For the calculation of Nu_L andNu_T one can use the correlations proposed for example in [6,8]. But the predictions with this correlation can deviate from the experimental data by 15–20%.

For more accurate calculations of the heat transfer more elaborate methods should be used based on solving the main conservation equations for the fluid flow, i.e. numerical methods. At the moment there are a number of commercial and special codes for hydrodynamic and thermohydraulic calculations which use different turbulence models for the closure of the main conservation equations. First of all, these are so-called k–ε and k–ω turbulence models and their modifications in which the transport equations are solved for the production of the turbulent energy (k) and its dissipation rate (ε) or turbulent frequency (ω). A correct choice of an appropriate turbulence model influences significantly the results of the calculations. In what follows the choice of the turbulence model will be discussed and the results of the numerical calculations will be compared with the experimental data.

3. Validation of turbulence models

The experimental data of Shehata and McEligot [9] were used for testing the turbulence models, which can be applied to the thermohydraulic simulation of the IFMIF/HFTM. These experiments have been performed to further investigate and understand the influence of strong heating on the ordinary gas internal flow. The experiments were conducted for air flowing upwards in a vertical circular tube. The inlet Reynolds numbers were about 6080, 6050 and 4260 with the non-dimensional heating rates, q^+ of 0.0018, 0.0035 and 0.0045, respectively, and these cases are classified as "essentially turbulent" (Run 618), "transitional or intermediate" (Run 635) and "laminarizing" (Run 445) [9]. The mean flow temperature and fields of mean axial velocity as well as the wall temperature along the heated section have been measured in all the cases. The boundary conditions and results of the measurements are presented in [9].

The cooling conditions of the IFMIF/HFTM differ to some extent from the conditions of these experiments.

The first difference is the difference in the hydraulic diameter of the HFTM cooling channels (~2 mm) and of the experimental section (27.4 mm). There are opinions in the literature [8] that the turbulence is suppressed in the channels with the hydraulic diameter less than 2 mm because of the small dimension of these channels. On the other hand, recent experiments [10] show the presence of turbulence in the channels with the hydraulic diameters $D_h \geqslant 0.7$ mm. So we conclude the existence of the turbulent flow in the IFMIF/HFTM channels under appropriate Reynolds numbers.

A small hydraulic diameter and a low pressure (0.3 MPa at the inlet) result in high flow velocity in the HFTM cooling channels. This enables one to neglect the buoyancy effect, and at the same time, one should take into account the gas compressibility that is negligible in the experiments of Shehata and McEligot [9].

In spite of these differences between the experiments and the cooling conditions of the HFTM, the data of the experiments are a very convenient case for the verification of the turbulence models considered for the thermohydraulic simulation of the IFMIF/HFTM. For examination we have taken several models offered by the commercial code STAR-CD [13]. All the models considered use the so-called Low Reynolds number treatment of the near wall layer which is regarded as an intensely inhomogeneous region. Standard High Reynolds number models, which apply the wall function based on the log-law relations, are unable to estimate correctly the influence of the near wall effects on the turbulence. To account for the near wall behaviour Low *Re* number models usually use empirical damping functions including some form of local *Re* number. The additional terms in the dissipation equation yield a correct level of the turbulence kinetic energy and its dissipation near the wall.

The first model is the linear Low-*Re*-number k–ε model (LLRM) of Lien et al. [14]. The linear turbulence models basically assume an isotropic turbulence structure and do not take into account the anisotropy of the turbulence caused by rapid flow acceleration. On the other hand, as shown by Torii and Yang [12] a high order turbulence model does not necessary work well, for example, for intermediate (“transitional”) conditions. If the linear models predict the velocity and pressure distribution well, then it is not necessary to use more complicated models. It is shown in [11] that one of the linear low-Reynolds number turbulence models developed by Launder and Sharma (LS) gives results which agree well with the experimental data. For instance, the disagreement between the predictions of the wall-to-bulk temperature difference and the data is not more than 6%. To estimate the contribution of the turbulence anisotropy to the relaminarization process, two non-linear turbulence models are employed. They present the expansion of the basically isotropic eddy-viscosity principle due to including non-linear strain–stress relations in the Reynolds stress equation. The first model is the non-linear (quadratic) extension of Lien’s turbulence model (QLRM). The second one is the k–ε model of Suga [16] with a cubic stress–strain correlation (CSLRM). A distinctive feature of these models is the functional dependence of C_μ on the strain parameter that additionally allows one to take into account the influence of the strain rate on the turbulent structure near the wall. The last model is the shear–stress-transport (SSTLRM) turbulence model [15]. This model combines the k–ε and k–ω turbulence models with the help of a blending function $F1$ that activates the k–ω model in the near wall region and the k–ε model for the rest of the flow. This model has the Low *Re* formulation, which does not require additional wall damping terms and very fine grid resolution of the near wall layer. The models above are presented in Appendix A.

To simulate the experiments the calculation domain was chosen consisting of the following sections: an adiabatic input section with the prescribed velocity profile and with a constant flow temperature at the inlet, a section with the assigned wall temperature taking into account the axial heat conduction in the channel wall, and a heated section with the assigned heat flux distribution on the wall. All assigned values are taken from the experiments [9].

The dependence of the air density on the temperature and pressure is described by the ideal gas equation of state. The dependence of the air dynamic viscosity, thermal conductivity and specific heat on temperature is taken from [8].

A grid influence study was conducted to determine how sensitive the Low *Re* number models might be to the near wall grid. The grid study involved running four cases for Run 635 with various values of the non-dimensional distance y^+ for the near wall cell and the number of grid cells located below a y^+ of 30, denoted as $N30$. The y^+ values varied from 0.2 to 1.5 and $N30$ varied from 10 to 40 for the unheated flow. For all cases, the grid nodes were equally spaced in the streamwise direction.

The turbulent dissipation rate ε near the wall was chosen as a criterion of grid sensitivity for k–ε turbulence models. For the SSTLRM the specific dissipation rate was chosen defined as $\omega \sim \varepsilon/k$. Fig. 2a shows the profiles of the turbulent dissipation rate versus y/R in the developed unheated flow. k–ε turbulence models show the similar behavior of ε depending on the grid resolution near the wall. $N30 \geqslant 16$ and $y^+ \leqslant 1$ for the near wall cell are required to adequately resolve the large gradient and maximum in the ε profile. More than 20 grid cells near the wall improve insignificantly the accuracy of the calculation but have an adverse effect on the stability of the calculation and considerably increases the CPU time. The axial wall temperature distribution in

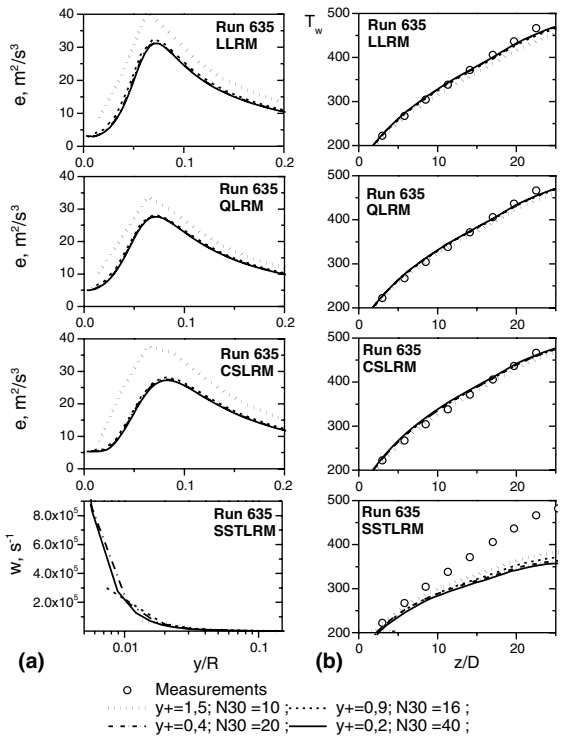

Fig. 2. Study of the sensitivity to near wall grid for Low *Re* number turbulence models: (a) profiles of turbulent dissipation rate ε for k–ε models and specific dissipation rate ω for the SST model normal to the wall ($z/D = 0$), (b) axial wall temperature distribution.

Fig. 2b shows that only in the case when $y^+ = 1.5$ and $N30 = 10$, the overestimation of the gradient and maximum of the turbulence dissipation rate near the wall causes the noticeable underprediction of the wall temperature. For the SSTLRM corresponding to the wall boundary conditions

$$\omega_w = \frac{6\nu_w}{0.075y^2},$$

ω decays very rapidly with the wall distance, and a coarser grid cannot resolve such a great variation of ω near the wall. Fig. 2 shows that in the cases of $y^+ = 1.5$ $N30 = 10$ and $y^+ = 0.9$ $N30 = 16$ the underestimation of the ω gradient leads to the suppressing of the turbulence in the near-wall region and causes the increasing of the predicted wall temperature. The grid $y^+ = 0.4$ $N30 = 22$ (800×75 cells), which is fine enough to obtain the correct behaviour of the turbulence characteristics near the wall was used for further calculations.

The comparison of such characteristics as the wall temperature and Stanton number, Fig. 3, shows that all the k–ε models give the results which are very close to the experimental data. The maximum disagreement (less than 5%) of the wall temperature is observed for Run 445, Fig. 3b. At the same time, the SSTLRM model predicts the wall temperature with the underestimation of ~20% for Run 635 and Run 445. One can see in Fig. 3a that the Stanton number predicted with the k–ε models correlates well with the experimental data and it deviates more and more from the turbulent value from Run 618 to Run 445. The SSTLRM model gives the results close to the turbulent value even for the laminarized Run 445.

All the models considered predict the pressure drop well except for Run 445, where a small underestimation is observed, Fig. 4. The velocity and temperature profiles of the flow at different channel cross-sections predicted with the k–ε models are also very close to the measurements. Fig. 5 shows the development of the mean axial velocity and the mean temperature calculated with the LLRM (QLRM and CSLRM give practically identical results). Only the SSTLRM model gives an appreciable deviation of the temperature profile at the end of the heated section, Fig. 6. So, the SSTLRM model predicts the experimental data worse than the k–ε models.

To understand this fact let us consider how Low Reynolds number corrections of the turbulence models can take into account the relaminarization phenomenon.

The transport equations of k–ε models include functions and coefficients which depend on the local Reynolds number $Re_t = k^2/\nu\varepsilon$ or Reynolds number like $Re_y = y\sqrt{k}/\nu$. First of all, this is the function f_μ that corrects the C_μ factor in the eddy-viscosity model ($C_\mu = 0.09$) and is introduced to mimic the direct effect of molecular viscosity on the turbulent shear stress. The turbulent shear stress near the wall being also reduced by the action of pressure fluctuation cannot be in principle correlated only by the Reynolds numbers Re_t, Re_y or y^+. Based on the measurements, the f_μ function thus attempts to simulate both the viscous and pressure strain effects, although it is properly correlated only for the former [17]. The drawback of this method can be the reason for the decrease in the accuracy of the k–ε models when the influence of the pressure forces on the Reynolds stresses caused by gas expansion becomes more noticeable as viscous effects (Run 445). The function f_μ has a predominant influence on the model performance. Additionally the extra terms in the dissipation equation like E in Suga's model or P'_k in Lien et al. model tend to increase the magnitude of the dissipation rate near the wall, which is also important for the relaminarization analysis. The SSTLRM model has a Low-*Re* formulation based on the Dirichlet boundary condition for ω in the near wall region $y^+ < 5$ and cannot take into account non-viscous damping effects at $y^+ > 5$.

The results of the calculation show the following (Fig. 7). The k–ε models give an insignificant increase in the peak of the turbulent kinetic energy at the end of the heated section ($z/D = 24.5$) for Run 618 only.

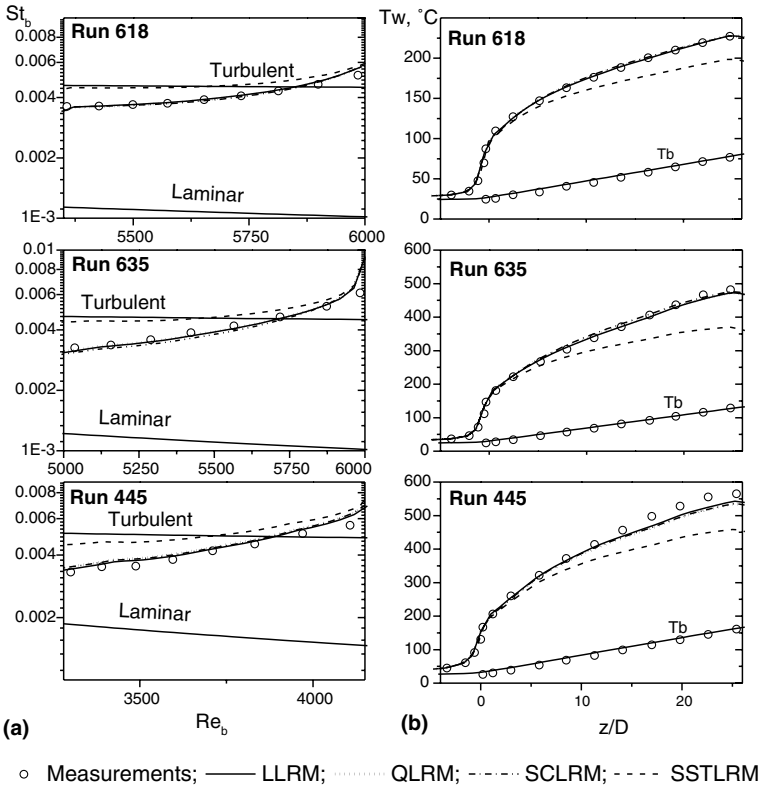

Fig. 3. Local Stanton number (a) and wall temperature compared (b) to measurements of Shehata and McEligot [9].

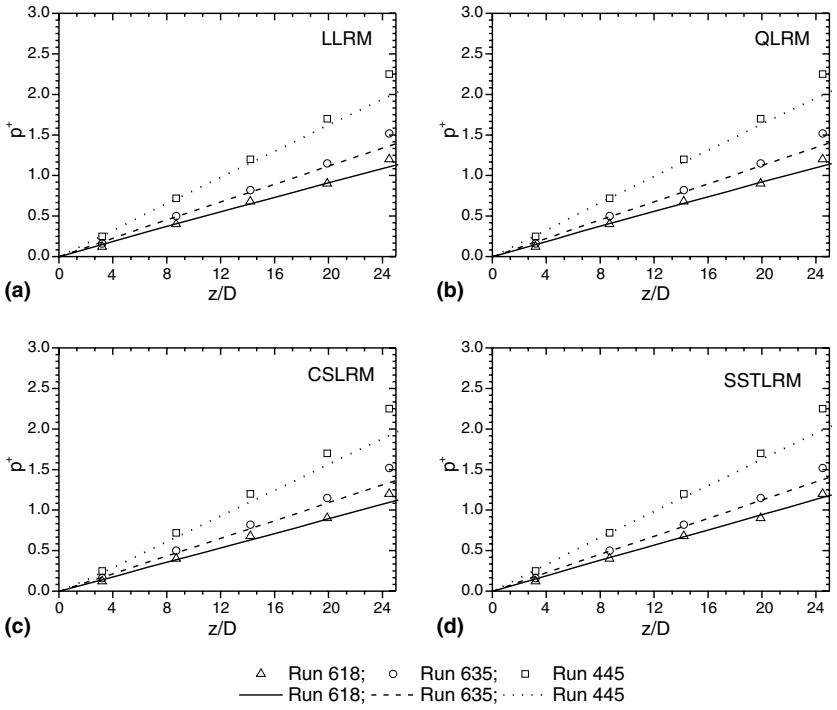

Fig. 4. Predicted pressure distribution compared to data from Shehata and McEligot [9].

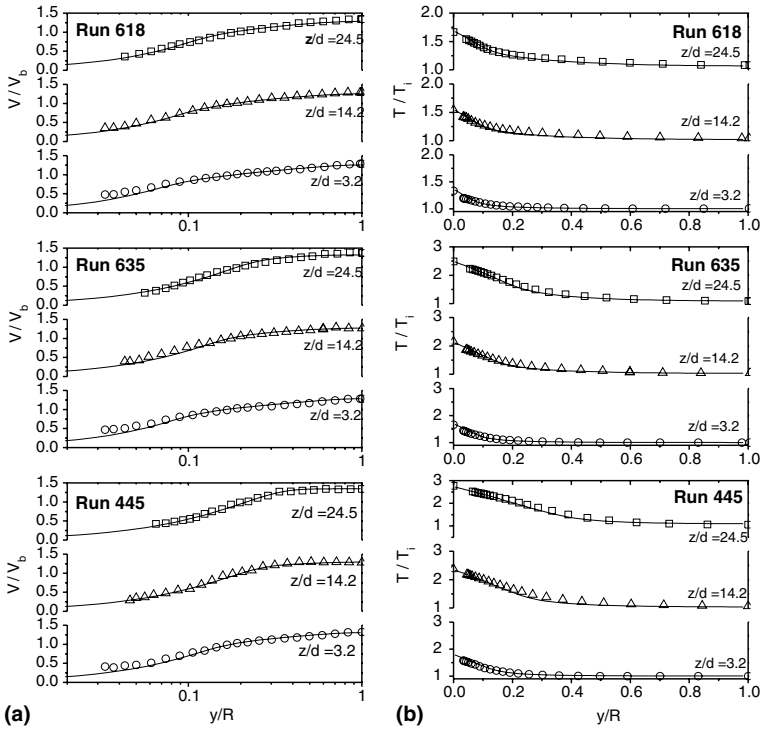

Fig. 5. Predicted axial development of mean axial velocity and mean temperature calculated with LLRM (lines) compared to measurements (symbols) of Shehata and McEligot [9].

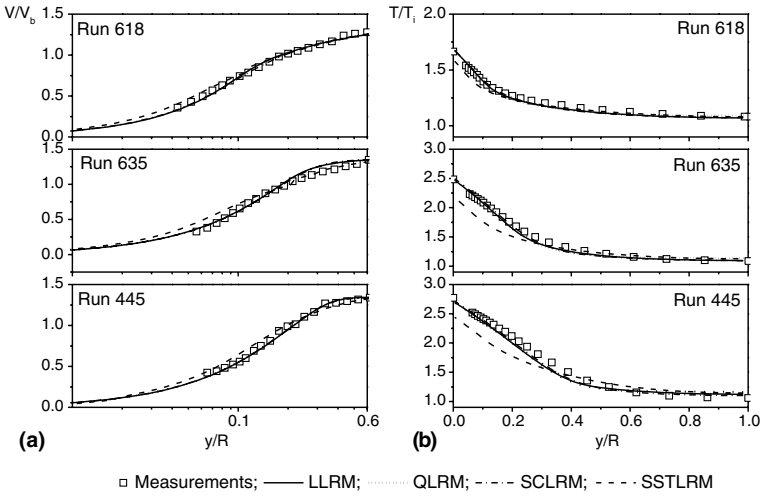

Fig. 6. Predicted (lines) axial development of mean axial velocity and mean temperature at $z/D = 25.4$ compared to measurements (symbols) of Shehata and McEligot [9].

They demonstrate a stable decrease in the turbulent kinetic energy along the heated section for Run 635 and Run 445. The peak of the turbulent kinetic energy moving to the flow centre along the heated length shows the increase in the viscous layer. This corresponds to the axial development of the turbulent viscosity, Fig. 8a–c. The SSTLR model shows in general a decrease in the turbulent kinetic energy level with the increase in the

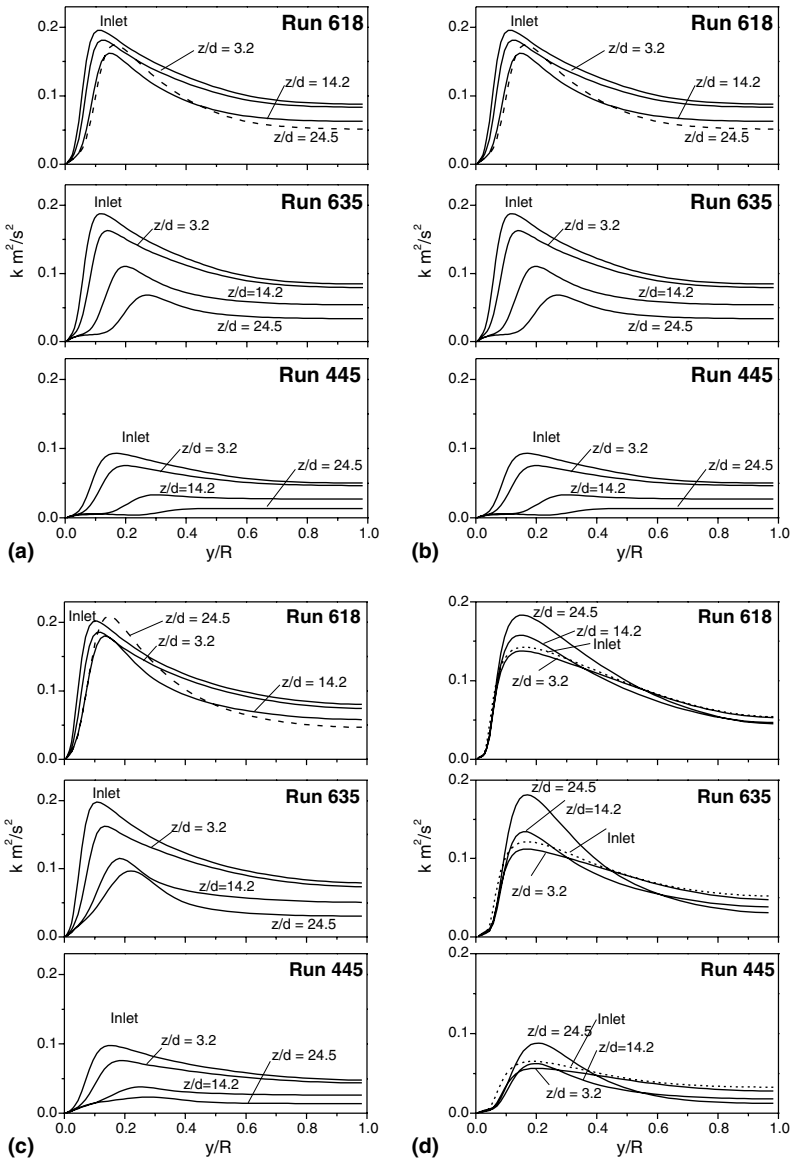

Fig. 7. Prediction of axial development of turbulent kinetic energy calculated with: (a) LLRM, (b) QLRM, (c) CSLRM, (d) SSTLRM.

heating rate, but it gives an increase in the peak of the turbulent kinetic energy along the heated section for all the runs. The model gives a very small increase in the viscous sub-layer thickness with the heating rate, Fig. 8d, and one can see in Fig. 7d that the peak of the turbulent kinetic energy does not practically move to the flow center, which does not correspond to our knowledge of the relaminarization mechanism.

Fig. 9 shows a significant difference in the Reynolds stress profiles given by the k–ε and the SSTLR models. The results obtained with the k–ε models show that the $\rho\overline{u'v'}$ profile becomes practically unchanged after $x/D = 14.2$ for Run 618 only, and continually varied along the heated section for Run 635 and Run 445. Such a character of the Reynolds stress behaviour was also reported in [9,11]. The SSTLR model demonstrates unchanged $\rho\overline{u'v'}$ profile after $x/D = 14.2$ for all the runs, giving excessive turbulent energy production.

Comparing the results obtained with linear and non-linear k–ε models one can say that there are no significant differences in the wall temperature and Stanton numbers given by the models. This means that the turbulence anisotropy plays an insignificant role in the case considered. Moreover, the fact that the viscosity

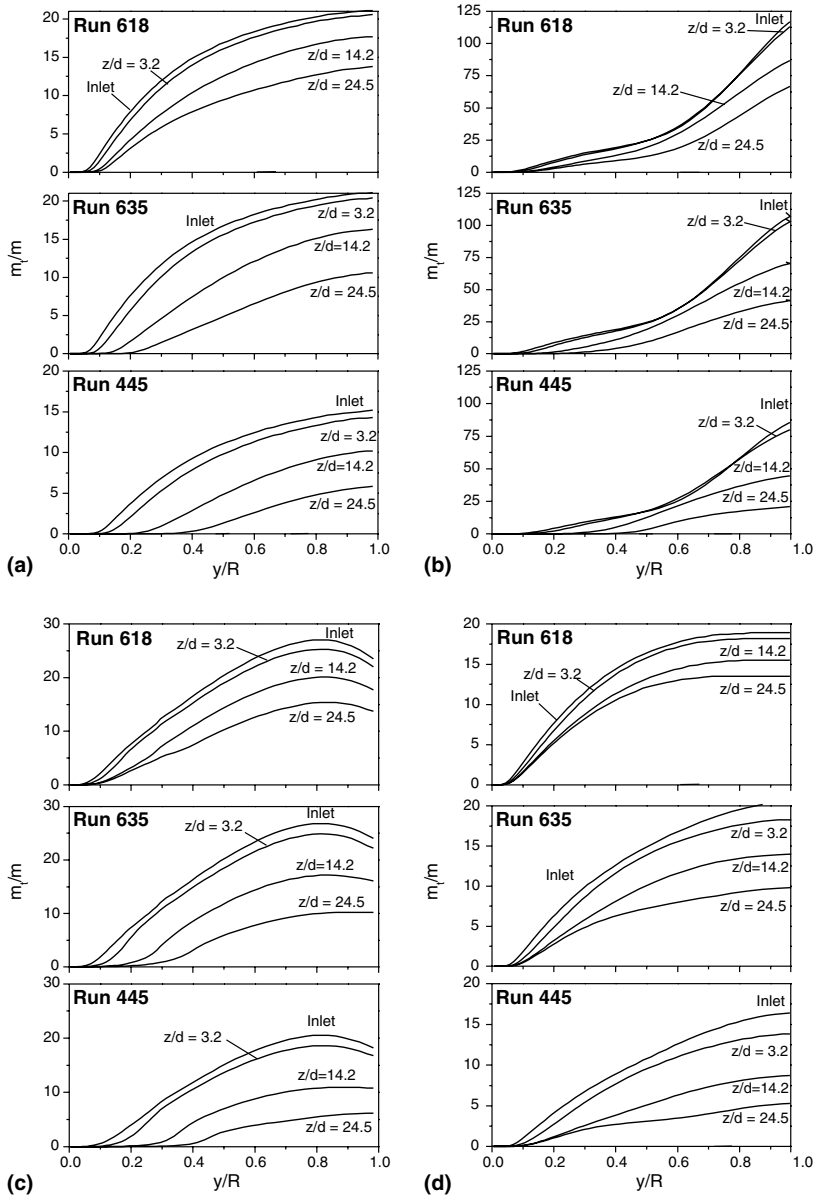

Fig. 8. Prediction of axial development of turbulent viscosity calculated with: (a) LLRM, (b) QLRM, (c) CSLRM, (d) SSTLRM.

coefficient C_μ becomes a function of the strain and vorticity parameters leads to the deformation of turbulent viscosity profile in the flow core. Such drawbacks of non-linear models were reported in [18], where it was pointed out that non-linear models can describe the turbulence characteristics incorrectly in the log-law region.

The results of the calculation also show that the non-linear models are very sensitive to the inlet data, they are less stable and are more time consuming. All these facts make the use of the non-linear turbulence models less attractive, especially for the tasks with a relatively simple geometry. So, the linear low Reynolds number turbulence model of Lien (LLRM) is chosen as more appropriate for the thermohydraulic analysis of the IFMIF high flux test module.

4. Numerical simulation of the IFMIF/HFTM with LLRM

The average temperature levels of 650 °C, 800 °C and 1025 °C in the volume with samples of the IFMIF/

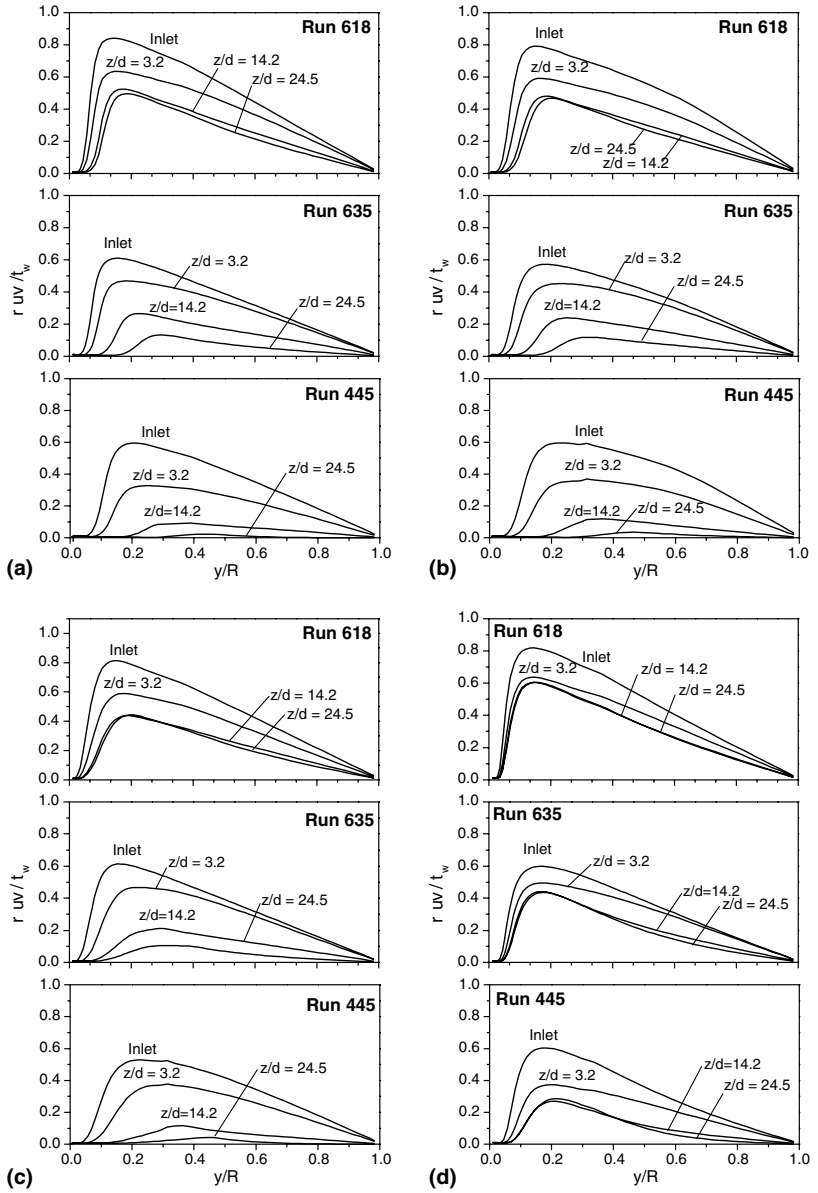

Fig. 9. Prediction of axial development of Reynolds stress calculated with: (a) LLRM, (b) QLRM, (c) CSLRM, (d) SSTLRM.

HFTM lead to the heat flux on the rig wall of 0.23 MW/m^2, 0.33 MW/m^2 and 0.43 MW/m^2, respectively (under the HFTM operation conditions). This corresponds to the non-dimensional heating rate q^+ of 0.0014, 0.0018 and 0.00235 in accordance with the boundary conditions for the HFTM, described in Section 1. The Reynolds number Re_b is equal to 8500, 8100 and 7800 for these cases at the Prandtl number (Pr_b) of 0.69. Using the criterion for the relaminarization in the form of $q^+ \geqslant 1.05 \times 10^{-6} \cdot Re_b^{0.8} \cdot Pr_b^{-0.6}$ [8] one can estimate the limit of the non-dimensional heating rate q^+_{limit} for each case and also estimate the probability of the relaminarization of the flow in the HFTM cooling channels. The results are the following.

$q^+ = 0.0014 < q^+_{limit} = 0.00182$
for the heat flux of 0.23 MW/m^2,
$q^+ = 0.0018 \approx q^+_{limit} = 0.00175$
for the heat flux of 0.33 MW/m^2,
$q^+ = 0.00235 > q^+_{limit} = 0.0017$
for the heat flux of 0.43 MW/m^2.

One can see that the flow relaminarization can occur in the case of heat flux equal to 0.33 MW/m^2 and 0.43 MW/m^2. The real value of q^+ is lower than the critical value of $q^+ = 0.003$, presented in Section 2.2, for all the cases considered, and probably the complete flow relaminarization will not take place even for the heat flux of 0.43 MW/m^2. Nevertheless, it is necessary to estimate the level of the influence of the flow relaminarization on the heat transfer in the HFTM cooling channels.

To investigate the influence of the heating intensity on the turbulence characteristics a two dimensional (2D) model of the HFTM cooling channel is elaborated and all the aforementioned cases are simulated with the boundary conditions in the form of the constant heat flux on the wall. We will refer to these cases as Run 223, Run 233 and Run 243, respectively (2 means 2D model; 0.23, 0.33, 0.43 are the heat flux values). The input data correspond to the HFTM operation conditions. The thermal conductivity in a solid structure is not taken into consideration and only half of the channel (because of its symmetry) is simulated. The model consists of 55×290 cells with $y^+ = 0.15$ for the near the wall cell. About 20 elements are placed in the region of $y^+ < 30$. The model includes an inlet section with the length of $x/D = 10$ and a heated section with the length of $x/D = 60$. The first calculations are done for the adiabatic flow (Fig. 10). The results of the calculation show that the thickness of the viscous sub-layer reaches its constant value before the section with heating, whereas a weak influence of the inlet hydraulic conditions on the profile of the turbulence characteristics in the flow core is observed at the beginning of the section with heating.

The results of the calculation of the flow with different heating intensities are discussed below. The diagrams of the velocity profile and turbulence characteristics of the flow are presented in Fig. 10. One can see a small increase in the viscous layer thickness for Run 223 and Run 233. The turbulent kinetic energy is continuously increased downstream and its value in the second half of the heated section is even higher than that for the adiabatic flow. Such behavior of the turbulent kinetic energy was mentioned by Bankston [5]. He explains that relatively high velocity fluctuations result from the temperature fluctuations. Comparing these results with the data in [9] we can note a different influence of the natural convection on the flow characteristics: the natural convection in IFMIF/HFTM cooling channels is negligible, whereas it suppresses the rise of the turbulent kinetic energy under the conditions of the experiments [9]. The Reynolds shear stress reaches a practically stable value after $x/D = 17.5$.

The process of the flow relaminarization for Run 243 is confirmed by all the turbulence characteristics. The thickness of the viscous sublayer continuously increases and the turbulent kinetic energy continuously decreases downstream. The variation of the $\rho\overline{u'v'}$ profile corresponds to the Reynolds stress variation in the experiment of McEligot and co-worker [9]. Only a relatively short heated length of the channel prevents the complete flow relaminarization. The integral flow characteristics such as the Nusselt number along the heated section and the Stanton number (Fig. 11) also confirm the flow relaminarization for Run 243.

To maintain the near-constant temperature in the volume with samples of the HFTM the electrical heating is required in addition to the nuclear heating. The axial nuclear heating gradient, the rise in the flow temperature along the heated section and the possibility of the flow relaminarization should be compensated for by a variable heating rate along the test section. Moreover, the heat conduction in a solid structure can also influence the heat transfer. To estimate the influence of the flow relaminarization on the temperature distribution in the volume with samples a 3D model of a capsule with samples was elaborated based on the reference design. Combining the nuclear and electrical heating, two cases were simulated corresponding to samples temperatures of 650 °C and 1025 °C, these cases are referred to as case 31 and case 32, respectively. For case 31 the heat flux on the cooling channel wall is practically constant and equal to 0.23 MW/m^2. For the case 32 an influence of the flow relaminarization on the heat transfer in the second half of the cooling channel must be compensate by decreasing of the electrical heating rate. As a result the heat flux on the channel wall is varied from the maximum value of 0.43 MW/m^2 at the beginning of the heated section to the minimum value of 0.35 MW/m^2 at the end of the heated section. The results of calculation show that the flow relaminarization is not observed in case 31, Fig. 12, though the intense heating and the gas compressibility have an adverse effect on the heat transfer. One can also see the effect of the flow relaminarization in case 32 resulting in an increase in the viscous sublayer and a decrease in the Reynolds stress, Fig. 12. While increasing in the first half of the heated section, the turbulent kinetic energy decreases in the second half of the section. The diagrams of the Nusselt and Stanton numbers, Fig. 13, show that they approach the laminar values.

For comparison, the calculations are repeated for cases 31 and 32 with constant properties of the gas, where the flow relaminarization is not taken into consideration. The axial temperature distributions in the volume with samples are shown in Fig. 14. One can see that the difference in the temperature values is not more than 25 °C in case 31, whereas it can exceed 50–80 °C in case 32. That means the influence of the flow relamina-

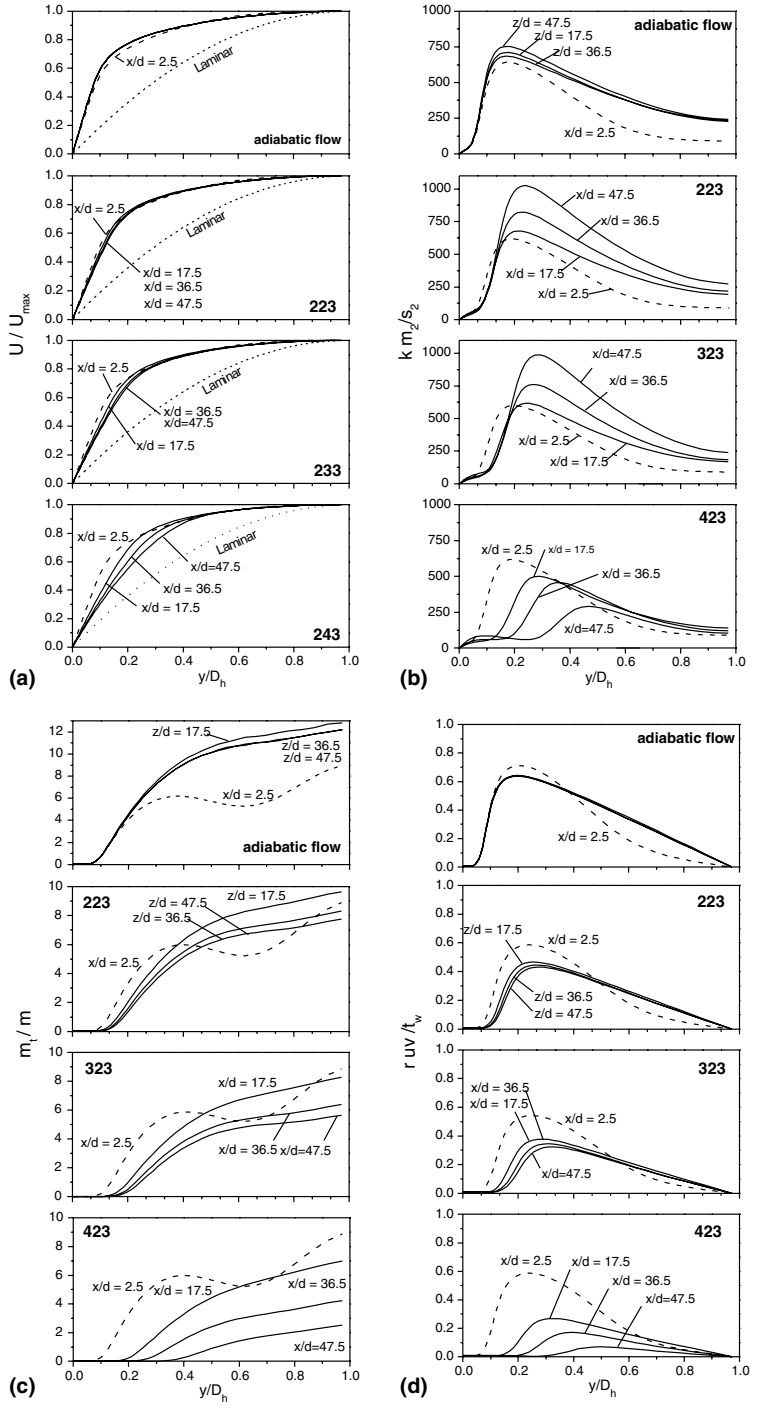

Fig. 10. Axial development of velocity profiles and turbulence quantities in the channel flow for the heat flux on the wall of 0.23, 0.33, 0.43 MW/m^2 calculated with 2D model of HFTM cooling channel: (a) normalized velocity profile, (b) turbulent viscosity, (c) turbulent kinetic energy, (d) Reynolds stress.

rization on the heat transfer for the temperature levels in the samples volume more then 650 °C cannot be ignored while choosing the operational loads of the IFMIF/HFTM.

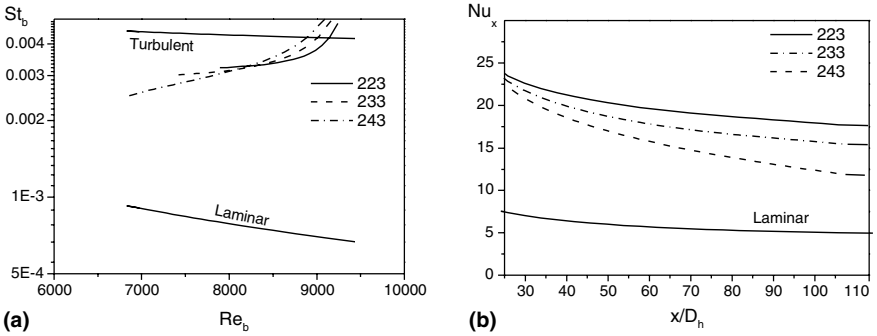

Fig. 11. The local Stanton number against the local bulk *Re* number (a) and axial distribution of the Nusselt number (b) calculated with 2D model of HFTM cooling channel.

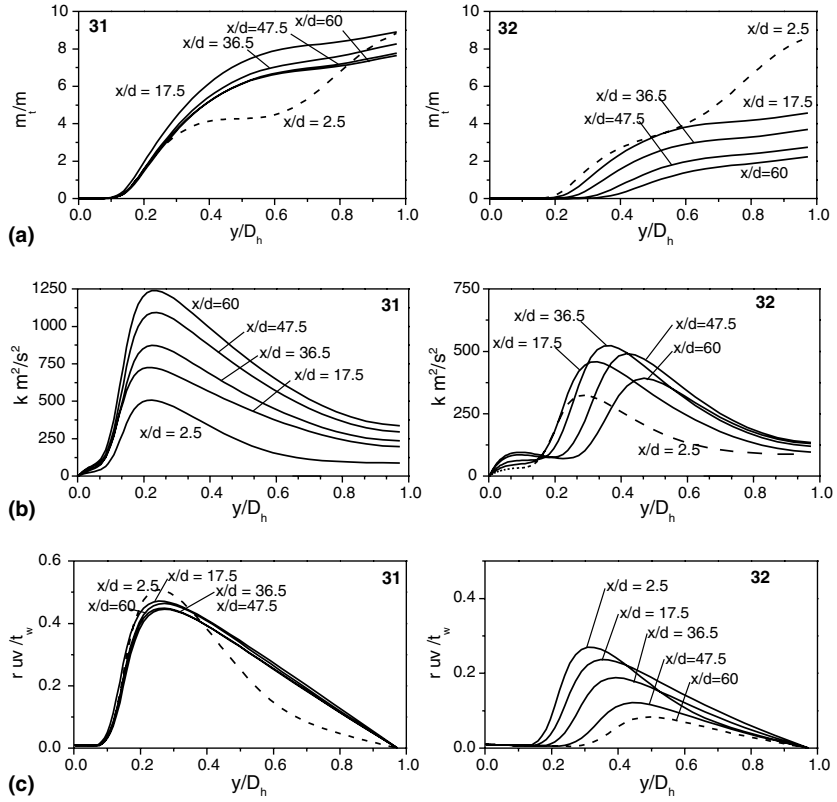

Fig. 12. Axial development of turbulence quantities in the middle cross-section of the channel flow calculated with 3D model of the HFTM rig: (a) turbulent viscosity, (b) turbulent kinetic energy and (c) Reynolds stress.

5. Summary

The analysis of the cooling conditions for the IFMIF/HFTM shows that partial flow relaminarization can take place under the geometry and operational conditions chosen (cooling channel width of 1 mm, low helium pressure of 0.3 MPa together with low Reynolds number $Re < 10{,}000$ and high heat flux up to 0.4 MW/m^2). This fact can result in a decrease in the heat transfer and increase in the temperature level in the samples tested. In this case the effect of the relaminarization should be accurately taken into consideration in thermo-hydraulic calculations because of the strong requirements for the temperature conditions in the volume with samples: a temperature range of 250–1000 °C with deviations of ±10–15 °C from the target value.

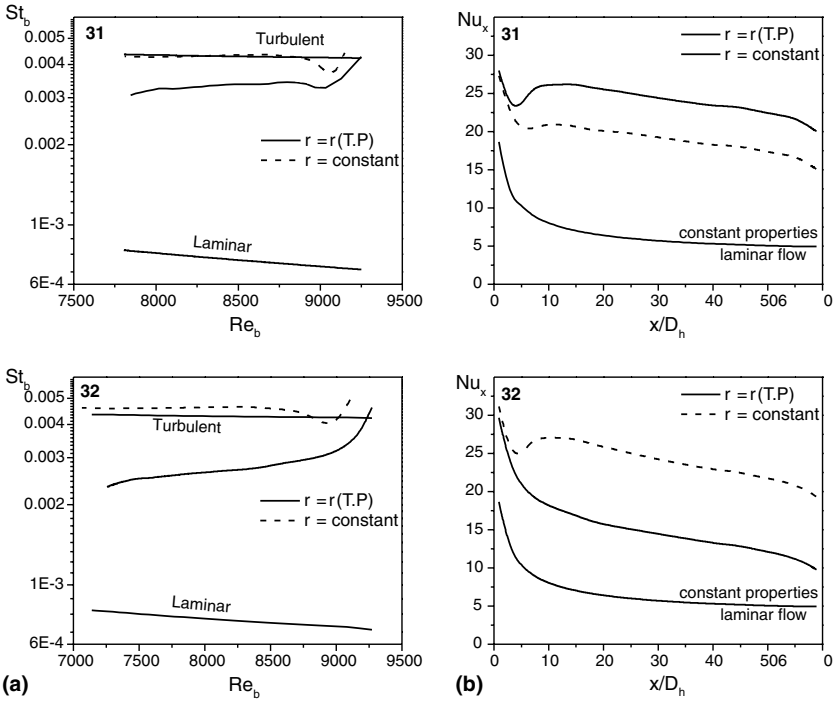

Fig. 13. The local Stanton number against the local bulk *Re* number (a) and axial distribution of the Nusselt number (b) in the middle cross-section of the channel flow calculated with 3D model of HFTM.

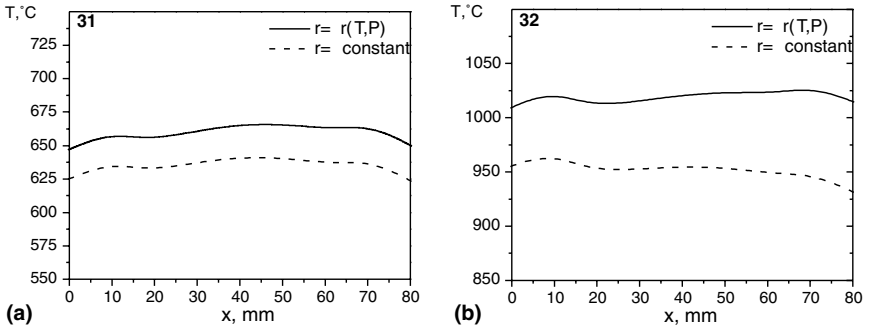

Fig. 14. Axial temperature distribution in specimens in the middle cross-section of the rig calculated with 3D model of HFTM.

Some of the empirical correlations presented in [6] take into account the influence of the intense heating on the heat transfer characteristics, but their applicability is restricted by the value of Prandtl and Reynolds numbers, the shape of the channel and its length, the type of boundary conditions and so on. For more accurate predictions of the heat transfer characteristics under the intense heating of the gas flow, the numerical methods should be used. The choice of an appropriate turbulence model is very important for this approach to correctly take into account the effect of the viscous layer development on the turbulent flow.

A comparison of different turbulence models offered by the STAR-CD code has been performed on the basis of the simulation of the experimental data of Shehata and McEligot [9]. This comparison showed that the low-Reynolds-number k–ε turbulence models predict the heat transfer characteristics close to the experimental data. This is due to the fact that these turbulence models provide a fairly good description of the development of the viscous layer in the geometrically simple channels under the conditions of flow acceleration caused by the gas expansion due to its intense heating. The linear k–ε turbulence model of Lien is adopted for the numerical simulation of the IFMIF/HFTM.

The experimental facility ITHEX (IFMIF Thermal–Hydraulic Experiment) is designed in the Forschungszentrum Karlsruhe (FZK) for a further detailed investigation of the heat transfer in the narrow channels and for an additional validation of the turbulence model chosen. The results of measurements and simulations will be reported in the next publication.

Acknowledgements

This work has been performed within the framework of the Nuclear Fusion Program of the Forschungszentrum Karlsruhe and is supported by the European Union within the European Fusion Technology Program.

The authors are grateful to Professor D.M. McEligot, University of Arizona, for providing the experimental data presented in Ref. [9].

Appendix A. Transport equations

A.1. k–ε Low Re number models

The turbulent viscosity μ_t is defined as

$$\mu_t = f_\mu \frac{C_\mu \rho k^2}{\tilde{\varepsilon}}; \quad C_\mu = 0.09 \tag{1}$$

For the turbulence energy k

$$\frac{\partial \rho k}{\partial t} + \frac{\partial \rho u_j k}{\partial x_j} = \frac{\partial}{\partial x_j}\left(\mu + \frac{\mu_t}{\sigma_k}\right)\frac{\partial k}{\partial x_j} + \rho P_k - \rho\varepsilon + \mu_t P_{NL} + \mu_t P_B \tag{2}$$

For the turbulence dissipation rate:

$$\frac{\partial(\rho\tilde{\varepsilon})}{\partial t} + \frac{\partial(\rho u_j \tilde{\varepsilon})}{\partial x_j} = \frac{\partial}{\partial x_j}\left(\mu + \frac{\mu_t}{\sigma_\varepsilon}\right)\frac{\partial \tilde{\varepsilon}}{\partial x_j} + C_{\varepsilon 1}\frac{\tilde{\varepsilon}}{k}P_k - C_{\varepsilon 2} f_2 \rho \frac{\tilde{\varepsilon}^2}{k} + C_{\varepsilon 3}\frac{\tilde{\varepsilon}}{k}\mu_t P_B + C_{\varepsilon 4}\rho\tilde{\varepsilon}\frac{\partial u_i}{\partial x_i} + C_{\varepsilon 1}\frac{\tilde{\varepsilon}}{k}\mu_t P_{NL} + E + S_\varepsilon \tag{3}$$

where

$\varepsilon = \tilde{\varepsilon} + D$

$\tilde{\varepsilon}$ the isotropic part of ε and is zero at the wall

$$P_k = \overline{u_i' u_j'}\frac{\partial u_i}{\partial x_j}$$

$$P_B \equiv -\frac{g_i}{\sigma_h}\frac{1}{\rho}\frac{\partial \rho}{\partial x_i}; \quad \sigma_h = 0.9$$

$$P_{NL} = -\frac{\rho}{\mu_t}\overline{u_i' u_j'}\frac{\partial u_i}{\partial x_j} - \left[2 s_{ij}\frac{\partial u_i}{\partial x_j} - \frac{2}{3}\left(\frac{\partial u_i}{\partial x_i} + \frac{\rho k}{\mu_t}\right)\frac{\partial u_i}{\partial x_i}\right]$$

$P_{NL} = 0$ for linear models

Yap correction S_ε (for CSLRM only):

$$S_\varepsilon = \max\left(0.83\frac{\tilde{\varepsilon}^2}{k}\left[\frac{k^{1.5}}{2.5\tilde{\varepsilon}y} - 1\right]\left[\frac{k^{1.5}}{2.5\tilde{\varepsilon}y}\right]^2, 0\right)$$

Model	Empirical coefficients							
	D	E	σ_k	σ_ε	$C_{\varepsilon 1}$	$C_{\varepsilon 2}$	$C_{\varepsilon 3}$	$C_{\varepsilon 4}$
LLRM/QLRM	0	0	1.0	1.22	$1.44(1 + P_k/P_k')$	1.92	1.44	−0.33
SCLRM	$2\nu\left(\frac{\partial\sqrt{k}}{\partial x_i}\right)$	$0.0022\frac{\widetilde{S}\mu_t k^2}{\tilde{\varepsilon}}\left(\frac{\partial^2 u_i}{\partial x_j \partial x_k}\right)^2$	1.0	1.22	1.44	1.92	1.44	−0.33

$P_k' = 1.33\left(1 - 0.3e^{-R_t^2}\right)\left[P_k + 2\mu\frac{k}{y^2}\right]e^{-0.00375 Re_y^2}$.

Model	Low-*Re* extensions		
	f_μ	f_1	f_2
LLRM/QLRM	$f_\mu = [1 - \exp(-0.0198 Re_y)]\left(1 + \frac{5.29}{Re_y}\right)$	1.0	$1 - 0.3e^{-Re_t^2}$
SCLRM	$f_\mu = 1 - \exp\left(\left(\frac{Re_t}{90}\right)^{0.5} - \left(\frac{Re_t}{400}\right)^2\right)$	1.0	$1 - 0.3e^{-Re_t^2}$

$Re_y = \frac{y\sqrt{k}}{\nu}$, $\quad Re_t = \frac{k^2}{\nu\varepsilon}$.

For non-linear models, the constitutive relations for the Reynolds stress are as follows:

$$\rho\frac{\overline{u_i'u_j'}}{k}=\frac{2}{3}\left(\frac{\mu_t}{k}\frac{\partial u_k}{\partial x_k}+\rho\right)\delta_{ij}-\frac{\mu_t}{k}S_{ij}+C_1\frac{\mu_t}{\varepsilon}\left[S_{ik}S_{kj}-\frac{1}{3}\partial_{ij}S_{kl}S_{kl}\right]+C_2\frac{\mu_t}{\varepsilon}\left[\Omega_{ik}S_{kj}+\Omega_{kl}S_{kl}\right]+C_3\frac{\mu_t}{\varepsilon}\left[\Omega_{ik}\Omega_{kj}-\frac{1}{3}\partial_{ij}\Omega_{kl}\Omega_{kl}\right]+C_4\frac{\mu_t}{\varepsilon^2}\left[S_{ki}\Omega_{lj}+S_{kj}\Omega_{li}\right]S_{kl}+C_5\frac{\mu_t}{\varepsilon^2}[S_{kl}S_{kl}-\Omega_{kl}\Omega_{kl}]S_{ij} \quad (4)$$

The mean strain and vorticity tensors, respectively are given by

$$S=\frac{k}{\varepsilon}\sqrt{\frac{1}{2}S_{ij}S_{ij}},\quad S_{ij}=\frac{\partial u_i}{\partial x_j}+\frac{\partial u_j}{\partial x_i}$$

$$\Omega=\frac{k}{\varepsilon}\sqrt{\frac{1}{2}\Omega_{ij}\Omega_{ij}},\quad \Omega_{ij}=\frac{\partial u_i}{\partial x_j}-\frac{\partial u_j}{\partial x_i}$$

$$\sigma_{k1}^{\omega}=1.176,\quad \sigma_{\omega1}^{\omega}=2,\quad \beta_1=0.075,$$

$$\beta_1^*=0.09,\quad \alpha_1=\frac{\beta_1}{\beta_1^*}-\frac{1}{\omega_{\omega1}^{\omega}}\frac{k^2}{\sqrt{\beta_1^*}},\quad k=0.41$$

$$\sigma_{k2}^{\omega}=1,\quad \sigma_{\omega2}^{\omega}=1.176,\quad \beta_2=0.0828,$$

$$\beta_2^*=0.09,\quad \alpha_2=\frac{\beta_2}{\beta_2^*}-\frac{1}{\omega_{\omega2}^{\omega}}\frac{k^2}{\sqrt{\beta_2^*}},\quad k=0.41$$

with

$$F_1=\tanh(\arg_l^4)$$

$$\arg_l=\min\left[\max\left(\frac{\sqrt{k}}{\beta^*\omega y};\frac{500\upsilon}{y^2\omega}\right);\frac{4\rho\sigma_{\omega2}^{\omega}k}{CD_{k\omega}y^2}\right]$$

$$CD_{k\omega}=\max\left(2\rho\sigma_{\omega2}^{\omega}\frac{1}{\omega}\frac{\partial k}{\partial x_j}\frac{\partial\omega}{\partial x_j};1.0e^{-10}\right)$$

$$S_{\omega}=2(1-F_1)\frac{1}{\omega_{\omega2}^{\omega}}\frac{1}{\omega_j}\frac{\partial\omega}{\partial x_j}\frac{\partial k}{\partial x_j}$$

turbulent viscosity

$$\mu_t=\rho\frac{a_1k}{\max(a_1\omega\Omega^*F_2)} \quad (7)$$

Model	Coefficients of k–ε constitutive relations					
	C_μ	C_1	C_2	C_3	C_4	C_5
QLRM	$\frac{0.667}{1.25+S+0.9\Omega}$	$\frac{0.75}{(1000+S^3)}$	$\frac{3.75}{(1000+S^3)}$	$\frac{4.75}{(1000+S^3)}$	0	0
SCLRM	$\frac{0.3[1-\exp(0.36\exp(0.75\eta))]}{1+0.35\eta^{1.5}}$	−0.1	0.1	0.26	$-10C_\mu^2$	$-5C_\mu^2$

$\eta=\max(S,\Omega)$.

A.2. SST model

For the turbulence energy k

$$\frac{\partial\rho k}{\partial t}+\frac{\partial\rho u_jk}{\partial x_j}=\frac{\partial}{\partial x_j}\left(\mu+\frac{\mu_t}{\sigma_k^{\omega}}\right)\frac{\partial k}{\partial x_j}+\rho P_k-\rho\beta^*k\omega \quad (5)$$

specific dissipation rate

$$\frac{\partial(\rho\omega)}{\partial t}+\frac{\partial(\rho u_j\omega)}{\partial x_j}=\frac{\partial}{\partial x_j}\left(\mu+\frac{\mu_t}{\sigma_{\omega}^{\omega}}\right)\frac{\partial\omega}{\partial x_j}+\rho\alpha\frac{\omega}{k}P_k-\rho\beta\omega^2+\rho S_{\omega} \quad (6)$$

for the SST model, the coefficients are expressed in the following general from

$$\Phi=F_1\Phi_1+(1-F_1)\Phi_2,$$

where Φ_1 and Φ_2 stand for the coefficients of the k–ω and the k–ε model respectively

where

$$a_1=0.31\quad \Omega^*=\sqrt{\frac{1}{2}\Omega_{ij}\Omega_{ij}}$$

$$F_2=\tanh(\arg_2^3)$$

$$\arg_2=\max\left(\frac{\sqrt{k}}{\beta^*\omega y};\frac{500\upsilon}{y^2\omega}\right)$$

References

[1] M. Martone (Ed.), IFMIF International Fusion Materials Irradiation Facility, Conceptual Design Activity, Final Report, IFMIF CDA TEAM, ENEA, Frascati. Report ENEA-RT/ERG/FUS/96.11, December 1996.

[2] S.J. Kline, W.C. Reynolds, F.A. Schraub, P.W. Runstadler, The structure of turbulent boundary layers, J. Fluid Mech. 30 (part 4) (1967) 741–773.

[3] B.E. Launder, Laminarization of the turbulent boundary layer by acceleration, Technical Report 77, MIT Gas Turbine Lab, 1964.
[4] R. Narasimha, K.R. Sreenivasan, Relaminarization of fluid flows, Adv. Appl. Mech. 19 (1979) 221–309.
[5] C.A. Bankston, The transition from turbulent to laminar gas flow in a heated pipe, J. Heat Transfer 1 (November) (1970) 569–578.
[6] D.M. McEligot, Convective heat transfer in internal gas flows with temperature-dependent properties, Adv. Transport Process. IV (1986) 114–199.
[7] V. Gnielinski, Ein neues Berechnungsverfahren für die Wärmeübertragung im Übergangsbereich zwischen laminarer und turbulenter Rohrströmung, Forschung in Ingenieurwesen—Eng. Res., B 61 (9) (1995).
[8] S. Kakac, R.K. Shah, W. Aung, Handbook of Single-phase Convective Heat Transfer, Wiley, 1987, pp. 4.2, 22.1.
[9] A. Mohsen Shehata, D.M. McEligot, Turbulence structure in the viscous layer of strongly heated gas flows, INEL-95/0223, Tech. Report, Idaho National Engineering Laboratory, November 1995.
[10] T.M. Adams, S.I. Abdel-Khalik, S.M. Jetter, An experimental investigation of single-phase forced convection in microchannels, Int. J. Heat Mass Transfer 41 (1998) 851–857.
[11] D.P. Mikielewicz, A. Mohsen Shehata, J.D Jackson, D.M. McEligot, Temperature, velocity and mean turbulence structure in strongly heated internal gas flows. Comparison of numerical predictions with data, Int. J. Heat Mass Transfer 45 (2002) 4333–4352.
[12] S. Torii, W. Yang, Laminarization of turbulent gas flow inside a strongly heated tube, Int. J. Heat Mass Transfer 40 (1997) 3105–3117.
[13] STAR-CD Version 3.15 User Guide, Computational Dynamics Limited, 2001.
[14] F.S. Lien, W.L. Chen, M.A. Leschziner, Low-Reynolds number eddy-viscosity modeling based on non-linear stress–strain/vorticity relations, Eng. Turbul. Model. Exp. 3 (1996).
[15] F.R. Menter, Two-equation eddy-viscosity turbulence models for engineering applications, AIAA J. 32 (8) (1994) 269–289.
[16] T.J. Craft, B.E. Launder, K. Suga, Development and application of a cubic eddy-viscosity model of turbulence, Int. J. Heat Fluid Flow 17 (1996) 108–115.
[17] V.C. Patel, W. Rodi, G. Scheuerer, Turbulence models for near-wall and low Reynolds number flows, AIAA J. 23 (9) (1985) 1308–1319.
[18] J. Piquet, Turbulent Flows. Models and Physics, Springer, 1999, p. 277.